

# Towards graphene plasmon-based free-electron infrared to X-ray sources

Liang Jie Wong<sup>1,2\*†</sup>, Ido Kaminer<sup>3\*†</sup>, Ognjen Ilic<sup>3</sup>, John D. Joannopoulos<sup>3</sup> and Marin Soljačić<sup>3</sup>

**Rapid progress in nanofabrication methods has fuelled a quest for ultra-compact photonic integrated systems and nanoscale light sources. The prospect of small-footprint, high-quality emitters of short-wavelength radiation is especially exciting due to the importance of extreme-ultraviolet and X-ray radiation as research and diagnostic tools in medicine, engineering and the natural sciences. Here, we propose a highly directional, tunable and monochromatic radiation source based on electrons interacting with graphene plasmons. Our complementary analytical theory and *ab initio* simulations demonstrate that the high momentum of the strongly confined graphene plasmons enables the generation of high-frequency radiation from relatively low-energy electrons, bypassing the need for lengthy electron acceleration stages or extreme laser intensities. For instance, highly directional 20 keV photons could be generated in a table-top design using electrons from conventional radiofrequency electron guns. The conductive nature and high damage threshold of graphene make it especially suitable for this application. Our electron-plasmon scattering theory is readily extended to other systems in which free electrons interact with surface waves.**

Graphene plasmons (GPs) exhibit extreme confinement of light with dynamic tunability<sup>1–6</sup>, making them promising candidates for electrical manipulation of light on the nanoscale<sup>7–13</sup>. By leveraging the high momentum of strongly confined GPs, we show that highly directional, tunable and monochromatic radiation at high frequencies can be produced from relatively low-energy electrons interacting with GPs. This design bypasses the need for lengthy electron acceleration stages or extreme laser intensities, allowing, for instance, highly directional 20 keV photons to be generated in a table-top design using electrons from conventional radiofrequency (RF) electron guns. The emission frequency is dynamically tunable via the electron energy, driving laser frequency or graphene doping. The prospect of a tunable, on-chip (ultraviolet) or table-top (X-ray) short-wavelength radiation source is especially exciting due to its potential applications as a research and diagnostic tool in medicine, engineering and the natural sciences<sup>14–17</sup>.

The GP-based free-electron radiation source we present here belongs to the category of compact, free-electron-driven radiation sources, which includes light wells<sup>18</sup>, Smith–Purcell emitters<sup>19–21</sup> and inverse Compton scattering sources<sup>22</sup>. GP-based emitters of short-wavelength radiation represent an unexplored avenue among the many promising applications that have sprung up around graphene<sup>23</sup>, a single-layer, honeycomb lattice of carbon atoms boasting incredible strength, extremely high electron mobility and the ability to support surface plasmon polaritons with a field confinement of over two orders of magnitude<sup>3,5,6,24</sup>. In recent years, great strides have been made in increasing the lifetime and confinement of graphene plasmons<sup>3,25</sup>. The confinement of GPs to plasmon wavelengths over 200 times smaller than the free-space wavelength has been predicted<sup>1,26–28</sup>, with very recent work suggesting that much higher confinements are also achievable<sup>29</sup>. Importantly, the observed plasmon lifetimes are gradually improving due to higher-quality samples and the fabrication of van der Waals heterostructures<sup>3</sup>, and are expected to increase further with

advances in fabrication techniques (for example, see ref. 30). Similar progress is also seen for GPs of shorter free-space wavelengths<sup>31</sup>, with reports of compelling evidence<sup>32</sup> and recent clear signatures<sup>33</sup> in the near-infrared. Observations are also anticipated in the visible regime<sup>4</sup>. This high confinement of GPs is key to the operation of our compact free-electron radiation source: strongly confined plasmons possess high momentum that allows for the generation of exceptionally high-energy output photons when electrons scatter off these plasmons. In this Article, we illustrate the concept of the GP-based compact free-electron radiation source with two examples: (1) highly directional hard X-ray generation from modestly relativistic electrons (at energies that do not require neutron shielding), and (2) a frequency conversion method with output that spans the infrared–visible–ultraviolet range, by using low-energy electrons that may conceivably be generated in an on-chip device. We also present a complete analytical theory for the GP–electron interaction that gives an excellent prediction of the radiation output as determined from our *ab initio* numerical simulations.

The mechanism behind the GP-based free-electron electromagnetic radiation source is illustrated schematically in Fig. 1a,b. A sheet of graphene on a dielectric substrate sustains a GP, excited by coupling a focused laser beam via a grating structure that is fabricated into the substrate, deposited on top of the graphene, or implemented as an array of graphene nanoribbons on the substrate<sup>25</sup>. When electrons are launched parallel to the graphene sheet, their subsequent interaction with the GP field induces transverse electron oscillations. The oscillations lead to the generation of short-wavelength, directional radiation. The radiation process (Fig. 1a) can be explained by the fact that plasmons are quasi-particles interacting with electrons according to the same fundamental rules that govern electron–photon interactions. However, the result is substantially different, because the plasmon’s dispersion relation, which lends itself to design and manipulation, can give the plasmon a much higher momentum than the photon at a given energy. In

<sup>1</sup>Department of Mathematics, Massachusetts Institute of Technology, 77 Massachusetts Avenue, Cambridge, Massachusetts 02139, USA.

<sup>2</sup>Singapore Institute of Manufacturing Technology, 2 Fusionopolis Way, Innovis, Singapore 138634, Singapore. <sup>3</sup>Department of Physics, Massachusetts Institute of Technology, 77 Massachusetts Avenue, Cambridge, Massachusetts 02139, USA. <sup>†</sup>These authors contributed equally to this work.

\*e-mail: kaminer@mit.edu; wonglj@simtech.a-star.edu.sg

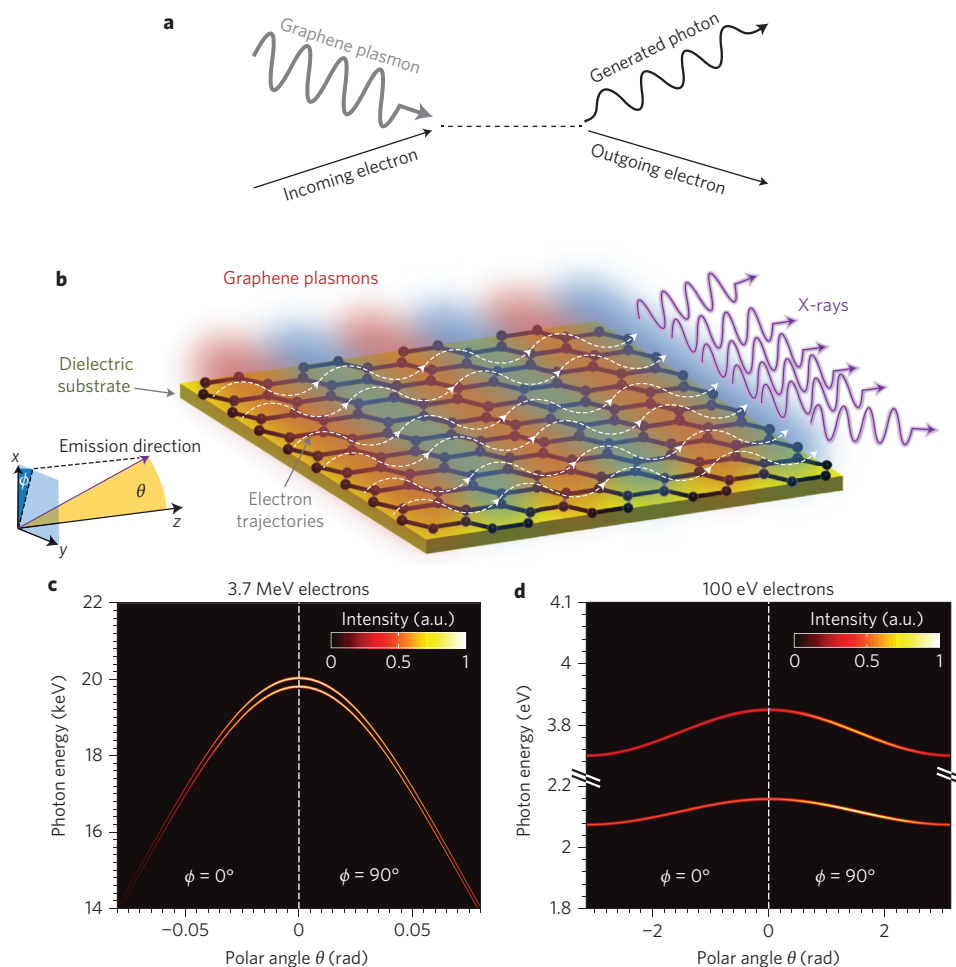


**Figure 1 | GP-based free-electron source of short-wavelength radiation.** **a,b**, Schematic showing the electron–plasmon interaction (**a**), in which free electrons (dotted white lines) interact with the graphene plasmon field (glowing red and blue bars) to produce short-wavelength output radiation (**b**). **c,d**, The resulting monochromatic radiation (purple lines in **b**) falls in the hard X-ray regime when modestly relativistic (3.7 MeV) electrons are used (**c**) and in the visible/ultraviolet regime when very non-relativistic (100 eV) electrons are used (**d**). The emission intensity is presented as a function of the polar angle of the outgoing radiation (horizontal) and its energy (vertical). The GP has a temporal frequency of  $2 \times 10^{14}$  Hz ( $\lambda_{\text{air}} = 1.5 \mu\text{m}$ ), in a graphene sheet that is electrostatically gated, or chemically doped, to have a spatial confinement factor of  $n = 180$ .

addition, plasmons have longitudinal field components that photons do not have. As a result, electron–plasmon scattering is distinct from the electron–photon scattering of the standard Thomson/Compton effect, opening up many possibilities not achievable with regular photons (see Supplementary Section 3 for a more detailed comparison).

To compute the output radiation, we performed multiparticle simulations of the GP–electron interaction, solving for the exact electron trajectories using the Newton–Lorentz equation, with the driving fields comprising both the GP and the field produced by the other electrons in the beam. Both near- and far-field inter-electron interactions are taken into account, as described in greater detail in Supplementary Section 6. The radiation spectrum is then a Fourier transform of the fields obtained from the Liénard–Wiechert potentials<sup>34</sup>. The GP fields are derived from a wavevector-dependent conductivity obtained within the random phase approximation (RPA)<sup>26,27</sup>. Figure 1b shows highly directional hard X-ray (20 keV) generation from 3.7 MeV electrons, which may be obtained readily from a compact RF electron gun (another example for different parameters is provided in Supplementary Section 8). This level of electron energy requirement obviates the need for further electron acceleration, for which huge facilities (for example, synchrotrons) are necessary. In addition, this scheme does not require the bulky and heavy neutron shielding

(which would add to the cost and complexity of the equipment and installation) that is necessary when electron energies above 10 MeV are used, as is often the case when X-rays are produced from free electrons in a Thomson or Compton scattering process. The resulting 20 keV photons in Fig. 1 are highly directional and monoenergetic, with an on-axis full-width at half-maximum (FWHM) energy spread of 0.25% and an angular spread of less than 10 mrad. The effect of electron beam divergence is discussed in Supplementary Section 5.

Figure 1d illustrates a completely different regime of operation, but based on the same physical mechanism, in which electrons with a kinetic energy of only 100 eV (a non-relativistic kinetic energy that can even be produced with an on-chip electron source) generate visible and ultraviolet photons at on-axis peak energies of 2.16 eV (0.32% spread) and 3.85 eV (0.2% spread). The lack of radiative directionality is an inevitable result of the lack of relativistic angular confinement when non-relativistic electrons are used.

In Fig. 1, the GP has a temporal frequency of  $\omega_0/2\pi = 2 \times 10^{14}$  Hz ( $\lambda_{\text{air}} = 1.5 \mu\text{m}$ ), in a graphene sheet that is electrostatically gated, or chemically doped, to have a carrier density of  $n_s = 3.2 \times 10^{13} \text{ cm}^{-2}$  (Fermi level of  $E_F = 0.66$  eV). This gives a GP spatial period of 8.33 nm (ref. 26), corresponding to a spatial confinement factor  $n$  (the ratio of the free-space wavelength to the GP wavelength) of

180. The graphene sheet is several micrometres in length, the interaction length being determined by the spatial size of the laser exciting the GP, which is 1.5  $\mu\text{m}$  long (FWHM).

Next, we turn to developing an intuitive analytical theory that explains the underlying physics behind the effects presented above. The theory offers an excellent prediction of both the frequency and the intensity of the radiation (see Fig. 2 for a comparison). The interaction between an electron and a GP can be analytically studied from a first-principles calculation of conservation laws, solving for the elastic collision of an electron of rest mass  $m$  and velocity  $v$  (normalized velocity  $\beta = v/c$ , Lorentz factor  $\gamma = (1 - \beta^2)^{-1/2}$ ) and a plasmon of energy  $\hbar\omega_0$  and momentum  $n\hbar\omega_0/c$ . Their relative angle of interaction is  $\theta_i$ , measured from the direction of the electron velocity. The output photon departing at angle  $\theta_f$  has energy  $\hbar\omega_{\text{ph}}$  and momentum  $\hbar\omega_{\text{ph}}/c$ , where  $\omega_{\text{ph}}$  is given by

$$\omega_{\text{ph}} = \omega_0 \frac{1 - n\beta \cos \theta_i - \frac{\hbar\omega_0}{\gamma mc^2} \frac{(n^2 - 1)}{2}}{1 - \beta \cos \theta_f + \frac{\hbar\omega_0}{\gamma mc^2} [1 - n \cos(\theta_f - \theta_i)]} \approx \omega_0 \frac{1 - n\beta \cos \theta_i}{1 - \beta \cos \theta_f} \quad (1)$$

The approximate equality—which neglects the effects of quantum recoil—holds whenever  $\gamma mc^2 \gg n\hbar\omega_0$ , which is always satisfied in our case. Note that the case of  $n=1$  reduces to the familiar formula for Thomson/Compton scattering, involving the relativistic Doppler shift of the radiation due to the interaction of an electron with a photon in free space.

A separate derivation based on classical electrodynamics (see Supplementary Sections 1 to 3 for details) corroborates the results of the above treatment. Assuming that the incident radiation excites a standing wave comprising counter-propagating GP modes—one of which co-propagates with the electrons—we find the output peak frequency as a function of device parameters and output angle  $\theta$

$$\omega_{\text{ph}\pm} = \frac{\omega_{\pm}}{1 - \beta \cos \theta} \quad (2)$$

where  $\omega_{\pm} = \omega_0(1 \pm n\beta)$  and  $\omega_0$  is the central angular frequency of the driving laser. In equation (2),  $\omega_{\text{ph}\pm}$  is due to electron interaction with the counter-propagating GP, whereas  $\omega_{\text{ph}\pm}$  is due to interaction with the co-propagating GP. Note that the rightmost expression in equation (1) reduces to  $\omega_{\text{ph}\pm}(\omega_{\text{ph}\pm})$  when  $\theta_i = \pi$  ( $\theta_i = 0$ ).

Furthermore, we found the spectrum of the emitted radiation as a function of its frequency  $\omega$ , azimuthal angle  $\phi$  and polar angle  $\theta$ , making the assumption of high confinement factors  $n \gg 1$  to achieve a completely analytical result:

$$\frac{d^2 I}{d\omega d\Omega} \approx \int dx dy W(x, y) \frac{Q^4 E_{0s}^2 \exp(-2Kx)L^2}{32\pi^2 \epsilon_0 c^5 m^2 n^2} \left( \frac{\omega}{\omega_0 \gamma} \right)^2 \times [U_+ \exp(\zeta_+) + U_- \exp(\zeta_-)] \quad (3)$$

where

$$U_{\pm} = \left\{ 1 + \sin^2 \theta \times \left[ \frac{\omega^2}{\omega_{\pm}^2} \beta^2 \cos^2 \phi + \left( \frac{1}{\gamma^4} - \cos^2 \phi \right) \left( 1 + \frac{\omega}{\omega_{\pm}} \beta \cos \theta \right)^2 \right] \right\} \left( \frac{\omega_0}{\omega_{\pm}} \right)^2 (\beta \pm \beta_g)^{-2} \quad (4)$$

and

$$\zeta_{\pm} = -\frac{L^2 [-\omega_{\pm} + \omega(1 - \beta \cos \theta)]^2}{c^2 n^2 (\beta \pm \beta_g)^2} \quad (5)$$

where  $\epsilon_0$  is the permittivity of free space,  $L$  is the spatial extent (intensity FWHM) of the GP,  $E_{0s}$  is the peak electric field amplitude on the graphene,  $\beta_g$  is the GP group velocity normalized to  $c$ ,  $K \approx n\omega_0/c$  is the GP out-of-plane wavevector,  $Q$  is the electron charge (although the theory holds for any charged particle), and  $W(x, y)$  is the electron distribution in the beam ( $x$  is the distance from the graphene, as in Fig. 1b). Note that the first and second terms between the square brackets of equation (3) correspond to spectral peaks associated with the counter-propagating ( $\omega_{\text{ph}\pm}$ ) and co-propagating ( $\omega_{\text{ph}\pm}$ ) parts of the standing wave, respectively, thus capturing the double-peak phenomenon observed in Fig. 1c,d. In deriving equation (3), we assumed, first, that transverse and longitudinal electron velocity modulations are small enough that  $\gamma$  is approximately constant throughout the interaction and, second, that the beam centroid is displaced negligibly in the transverse direction, both of which are very good approximations in most cases of interest (Fig. 2). Details of the derivation are provided in Supplementary Sections 1 to 3, where we address the general problem of radiation scattered by electrons interacting with GP modes of arbitrary  $n$  (not just  $n \gg 1$ ). There, we also derive an expression for the threshold beyond which our approximations break down due to ponderomotive deflection (Supplementary Section 7). This discrepancy is shown in Fig. 2b and becomes negligible when the GP strength is decreased, as in Fig. 2c. The excellent agreement between the analytical results and exact numerical calculations (Fig. 2) demonstrates the validity of our electron-GP scattering theory.

An overview of the different frequency conversion regimes of GP-based free-electron radiation sources is presented in Fig. 3. Lines corresponding to confinement factors  $n = 50, 180, 300$  and  $1,000$  are shown in each diagram ( $n = 1$  is also shown for reference). Figure 3a shows that non-relativistic electrons available from the very common scanning electron microscope (SEM)—the leftmost regime—are already sufficient for hard ultraviolet and soft X-ray generation. Semi-relativistic electrons, such as those used in transmission electron microscopes (TEMs), allow the generation of soft X-rays from infrared GPs (for example, 340 eV photons from 200 keV electrons). The next regime of electron energies—modestly relativistic electrons achievable in RF guns—is sufficient to generate hard X-rays, circumventing the need for additional sophisticated acceleration stages, which are necessary to produce the highly relativistic electrons (rightmost regime) usually required in most free-electron-based X-ray generation schemes. Considering only GP parameters that have already been demonstrated experimentally<sup>3</sup>, we note that 4 keV X-ray photons are attainable with 5 MeV electron beams using far-infrared ( $\lambda_{\text{air}} = 10 \mu\text{m}$ ) GPs with a confinement factor of  $n = 150$ . (In Supplementary Section 8, we present an investigation at  $\lambda_{\text{air}} = 10 \mu\text{m}$ , showing that such plasmons can already generate few-keV X-rays with 3.7 MeV electrons.) It should be noted that the Fermi energy of graphene provides a robust means of tuning the output photon energy. As shown in Supplementary Section 3, we can vary the output photon energy from 30 keV to over 60 keV just by tuning the Fermi energy from 0.5 to 0.9 eV (assuming 6 MeV electrons). This is in addition to the tunability that is already achievable by controlling the electron energy and the frequency of the driving laser.

Figure 3b shows the regime of non-relativistic electron energies. Frequency-doubling is already attainable with few-electronvolt electrons (for example, 2.8 eV when  $n = 300$ ). Several tens of volts will allow a much higher upconversion, which can convert infrared

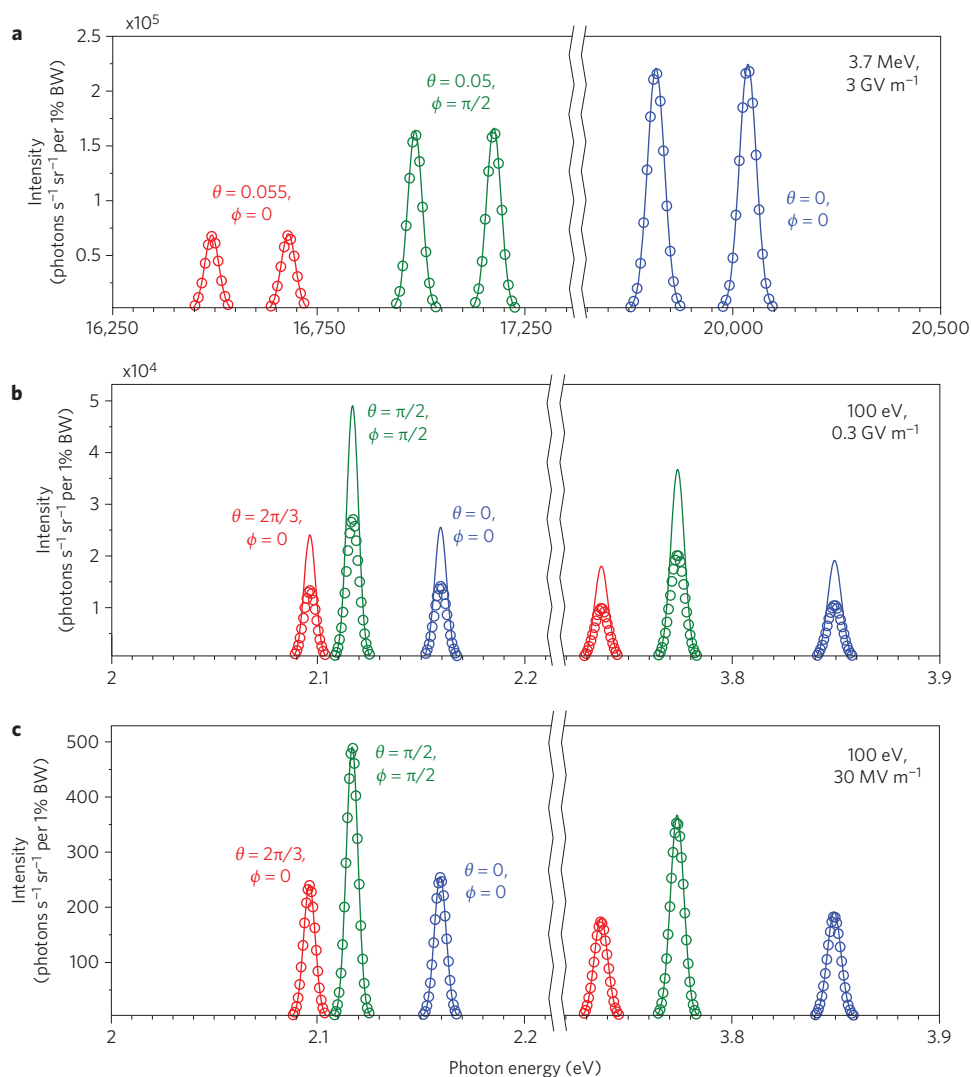


**Figure 2 | Numerical versus analytical results of the radiation spectrum. a–c**, Numerically (circles) and analytically (solid lines) computed radiation intensities in units of photons per second per steradian per 1% bandwidth (BW) for 3.7 MeV electrons with a peak electric field amplitude of  $E_{0s} = 3 \text{ GV m}^{-1}$  on the graphene surface (as in Fig. 1c) (**a**), 100 eV electrons with  $E_{0s} = 0.3 \text{ GV m}^{-1}$  (as in Fig. 1d) (**b**) and 100 eV electrons with  $E_{0s} = 30 \text{ MV m}^{-1}$  (**c**). The radiation spectra correspond to an average current of 100  $\mu\text{A}$ . The electron beam is centred 5 nm from the graphene sheet and has a transverse distribution of standard deviation 10 nm. All GP parameters are as in Fig. 1. The different colours represent measurements from different angles.

plasmons to visible or ultraviolet wavelengths. Figure 3b also presents the possibility of frequency downconversion.

Graphene is especially suited to our purpose because of its combination of metallic and dielectric properties: it can support electric fields stronger than any metal and even comparable to those supported by dielectric structures<sup>22,35</sup>, while its high conductivity prevents the charge accumulation that might otherwise hinder its usability. For example, the peak electric field amplitude of  $3 \text{ GV m}^{-1}$  on the graphene assumed in Fig. 2a is below the graphene breakdown threshold<sup>36</sup>. We expect higher fields to be achievable for shorter pulses, increasing the efficiency of our approach. The expected losses of GPs are also averted in our design because of the micrometre-scale interaction length and the method of excitation (Supplementary Section 4).

A central and novel advantage of our scheme is the ability to harness relatively low-energy electrons for the generation of tunable, highly directional, high-energy radiation in a compact design. The unavoidable price of using such low-energy electrons is a decrease in output radiation. The output intensity (equation (3)) typically scales as  $\gamma^2$  for relativistic electrons, because the factor  $\omega/\gamma\omega_0$  scales as  $\gamma$  at the on-axis intensity peak ( $\theta \approx 0^\circ$ ) when

$\beta \approx 1$ . This prevents the photon yield of our system ( $\gamma \approx 1\text{--}10$ ) from being comparable to that of large X-ray facilities ( $\gamma \gg 1$ ), which use highly relativistic electrons and large interaction lengths. Nevertheless, the GP-based free-electron radiation source will be useful for table-top laboratory and clinical applications that require only modest intensities. Greater photon flux may be achieved by pre-bunching the electrons<sup>37,38</sup>, thereby creating a periodic electron distribution that radiates coherently. The resulting output intensity is enhanced by a factor of  $N$ , the number of electrons in each bunch. Another method for enhancing the emission involves a multilayer configuration in which multiple versions of the structure in Fig. 1b are vertically stacked above one another. Such a configuration relaxes constraints on the size of the electron beam in the  $x$  dimension, allowing larger currents to be used. Specific multilayer configurations can also enhance the GP intensity and its coupling efficiency to the excitation pulse<sup>39</sup>. Recent advances in the fabrication of graphene heterostructures<sup>40–42</sup> have demonstrated the feasibility of such multilayer structures. The interaction time may also be increased by using longer sheets of graphene (for example, obtained using chemical vapour deposition instead of exfoliation). Equation (3) predicts substantial

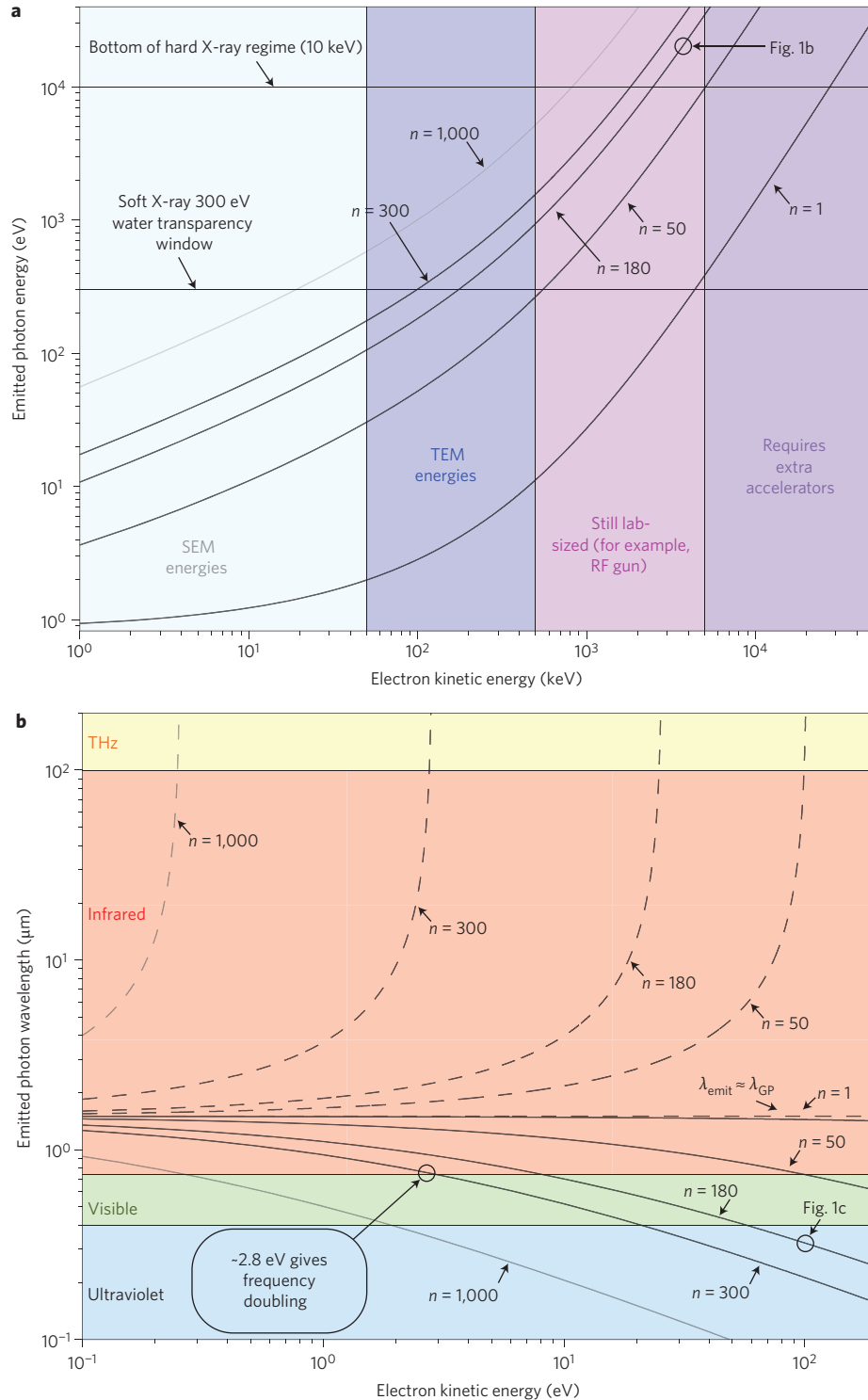


**Figure 3 | Regimes of frequency conversion for the GP-based free-electron radiation source.** **a**, Soft and hard X-ray generation using electron beams of energies achievable with laboratory-sized equipment, without extra acceleration stages. **b**, Schemes for frequency upconversion (continuous black lines) and downconversion (dashed black lines) using a source of very non-relativistic electrons, which can be implemented in on-chip configurations. Notice that extreme downconversion occurs at the point where the electron velocity matches the GP phase velocity and electron-plasmon coupling is enhanced. The assumed free-space wavelength is  $1.5 \mu\text{m}$  for both panels (as equation (1) shows, the vertical axes scale linearly when a different wavelength is used).

improvements in output intensity, energy spread and collimation with longer interaction lengths. Finally, high-quality, flat electron sheets in the  $z$ - $y$  plane<sup>43,44</sup> would allow for greater overlap between the electron beam and the GP. This is evidenced by equation (3), where the exponential pre-factor  $\exp(-2Kx)$  arises because the GP is a surface mode. We elaborate further on

methods to enhance the brightness of the GP radiation source in Supplementary Section 9.

In conclusion, we have presented a novel concept of a compact, tunable, highly directional radiation source based on electron beams interacting with GPs. The small scale of the source, together with the CMOS compatibility of graphene, makes it promising for on-chip

integration. Such a device would feature exceptional tunability—spanning the electromagnetic spectrum from infrared to hard X-ray frequencies—that is controllable in three ways: by varying the electron energy, the frequency of the surface plasmon, and the graphene doping (for example, by electrical gating). Like metals, the conductive nature of graphene keeps it from accumulating charges that might disrupt its operation, and like regular dielectrics graphene can survive relatively high field amplitudes. These qualities, coupled with the high confinement factors—and hence small spatial periodicity—of GPs, make graphene a promising platform upon which to realize chip-scale light sources with low-energy electrons, circumventing the use of additional acceleration stages. Interestingly, recent work has already demonstrated large-gradient on-chip acceleration<sup>35,45,46</sup>, which if successfully scaled up could create highly compact few-MeV accelerators, thus making even the hard X-ray graphene-based source accessible on chip. The GP-based free-electron radiation source offers a rich field for further exploration. Methods of improving the photon yield include adding multiple layers and increasing the length of the GP, hence increasing the number of interaction cycles. The prospect of a GP-based free-electron laser, in which the radiation output causes the electrons to bunch coherently via self-amplified spontaneous emission<sup>20,35,47</sup>, is also an interesting topic for future research. In general, electrons can also excite plasmons<sup>48,49</sup>, which might back-react on them and influence both the radiation emission and the plasmon emission. In this work, we have concentrated on the regime where these effects are of higher order and can be neglected. Looking beyond graphene, the concept presented here is applicable to other two-dimensional materials that support surface plasmons. Examples include bilayer graphene<sup>50</sup> and single atomic layers of silver and gold, which have been shown in very recent works to have high confinement factors while also having higher frequencies than GPs<sup>1</sup>.

Received 21 April 2015; accepted 8 October 2015;  
published online 23 November 2015

## References

- Jablan, M., Soljagic, M. & Buljan, H. Plasmons in graphene: fundamental properties and potential applications. *Proc. IEEE* **101**, 1689–1704 (2013).
- Koppens, F. H. L., Chang, D. E. & de Abajo, F. J. G. Graphene plasmonics: a platform for strong light–matter interactions. *Nano Lett.* **11**, 3370–3377 (2011).
- Woessner, A. *et al.* Highly confined low-loss plasmons in graphene–boron nitride heterostructures. *Nature Mater.* **14**, 421–425 (2015).
- De Abajo, F. J. G. Graphene plasmonics: challenges and opportunities. *ACS Photon.* **1**, 135–152 (2014).
- Fei, Z. *et al.* Gate-tuning of graphene plasmons revealed by infrared nano-imaging. *Nature* **487**, 82–85 (2012).
- Chen, J. *et al.* Optical nano-imaging of gate-tunable graphene plasmons. *Nature* **487**, 77–81 (2012).
- Alonso-González, P. *et al.* Controlling graphene plasmons with resonant metal antennas and spatial conductivity patterns. *Science* **344**, 1369–1373 (2014).
- Yao, Y. *et al.* Broad electrical tuning of graphene-loaded plasmonic antennas. *Nano Lett.* **13**, 1257–1264 (2013).
- Fang, Z. *et al.* Plasmon-induced doping of graphene. *ACS Nano* **6**, 10222–10228 (2012).
- Yan, H. *et al.* Damping pathways of mid-infrared plasmons in graphene nanostructures. *Nature Photon.* **7**, 394–399 (2013).
- Ju, L. *et al.* Graphene plasmonics for tunable terahertz metamaterials. *Nature Nanotech.* **6**, 630–634 (2011).
- Grigorenko, A. N., Polini, M. & Novoselov, K. S. Graphene plasmonics. *Nature Photon.* **6**, 749–758 (2012).
- Low, T. & Avouris, P. Graphene plasmonics for terahertz to mid-infrared applications. *ACS Nano* **8**, 1086–1101 (2014).
- Lukianova-Hleb, E. Y. *et al.* On-demand intracellular amplification of chemoradiation with cancer-specific plasmonic nanobubbles. *Nature Med.* **20**, 778–784 (2014).
- Bargheer, M., Zhavoronkov, N., Woerner, M. & Elsaesser, T. Recent progress in ultrafast X-ray diffraction. *ChemPhysChem* **7**, 783–792 (2006).
- Rousse, A. *et al.* Femtosecond X-ray crystallography. *Rev. Mod. Phys.* **73**, 17–31 (2001).
- Bressler, C. & Chergui, M. Ultrafast X-ray absorption spectroscopy. *Chem. Rev.* **104**, 1781–1812 (2004).
- Adamo, G. *et al.* Light well: a tunable free-electron light source on a chip. *Phys. Rev. Lett.* **104**, 024801 (2010).
- Smith, S. J. & Purcell, E. M. Visible light from localized surface charges moving across a grating. *Phys. Rev.* **92**, 1069 (1953).
- Friedman, A., Gover, A., Kurizki, G., Ruschin, S. & Yariv, A. Spontaneous and stimulated emission from quasifree electrons. *Rev. Mod. Phys.* **60**, 471–535 (1988).
- Gover, A., Dvorkis, P. & Elisha, U. Angular radiation pattern of Smith–Purcell radiation. *J. Opt. Soc. Am. B* **1**, 723–728 (1984).
- Karagodsky, V., Schieber, D. & Schächter, L. Enhancing X-ray generation by electron-beam–laser interaction in an optical Bragg structure. *Phys. Rev. Lett.* **104**, 024801 (2010).
- Geim, A. K. Graphene: status and prospects. *Science* **324**, 1530–1534 (2009).
- Zhou, W. *et al.* Atomically localized plasmon enhancement in monolayer graphene. *Nature Nanotech.* **7**, 161–165 (2012).
- Brar, V. W., Jang, M. S., Sherrott, M., Lopez, J. J. & Atwater, H. A. Highly confined tunable mid-infrared plasmonics in graphene nanoresonators. *Nano Lett.* **13**, 2541–2547 (2013).
- Jablan, M., Buljan, H. & Soljagic, M. Plasmonics in graphene at infrared frequencies. *Phys. Rev. B* **80**, 245435 (2009).
- Hwang, E. H. & Das Sarma, S. Dielectric function, screening, and plasmons in two-dimensional graphene. *Phys. Rev. B* **75**, 205418 (2007).
- Wunsch, B., Sauber, T., Sols, F. & Guinea, F. Dynamic polarization of graphene at finite doping. *New J. Phys.* **8**, 318 (2006).
- Page, A. F., Ballout, F., Hess, O. & Hamm, J. M. Nonequilibrium plasmons with gain in graphene. *Phys. Rev. B* **91**, 075404 (2015).
- Liu, G. *et al.* Epitaxial graphene nanoribbon array fabrication using BCP-assisted nanolithography. *ACS Nano* **6**, 6786–6792 (2012).
- Brar, V. W. *et al.* Observation of carrier-density-dependent many-body effects in graphene via tunneling spectroscopy. *Phys. Rev. Lett.* **104**, 036805 (2010).
- Zhang, Q. *et al.* Graphene surface plasmons at the near-infrared optical regime. *Sci. Rep.* **4**, 6559 (2014).
- Tielrooij, K. J. *et al.* Electrical control of optical emitter relaxation pathways enabled by graphene. *Nature Phys.* **11**, 281–287 (2015).
- Jackson, J. D. *Classical Electrodynamics* 2nd edn (Wiley, 1975).
- England, R. J. *et al.* Dielectric laser accelerators. *Rev. Mod. Phys.* **86**, 1337 (2014).
- Roberts, A. *et al.* Response of graphene to femtosecond high-intensity laser irradiation. *Appl. Phys. Lett.* **99**, 051912 (2011).
- Graves, W. S., Kärtner, F. X., Moncton, D. E. & Piot, P. Intense superradiant X rays from a compact source using a nanocathode array and emittance exchange. *Phys. Rev. Lett.* **108**, 263904 (2012).
- Nanni, E. A., Graves, W. S. & Moncton, D. E. Nano-modulated electron beams via electron diffraction and emittance exchange for coherent X-ray generation. Preprint at <http://arXiv:1506.07053> [physics.acc-ph].
- Stauber, T. & Gómez-Santos, G. Plasmons and near-field amplification in double-layer graphene. *Phys. Rev. B* **85**, 075410 (2012).
- Yu, W. J. *et al.* Highly efficient gate-tunable photocurrent generation in vertical heterostructures of layered materials. *Nature Nanotech.* **8**, 952–958 (2013).
- Georgiou, T. *et al.* Vertical field-effect transistor based on graphene–WS<sub>2</sub> heterostructures for flexible and transparent electronics. *Nature Nanotech.* **8**, 100–103 (2013).
- Britnell, L. *et al.* Field-effect tunneling transistor based on vertical graphene heterostructures. *Science* **335**, 947–950 (2012).
- Brinkmann, R., Derbenev, Y. & Flöttmann, K. A low emittance, flat-beam electron source for linear colliders. *Phys. Rev. Spec. Top.-Ac.* **4**, 053501 (2001).
- Piot, P., Sun, Y.-E. & Kim, K.-J. Photoinjector generation of a flat electron beam with transverse emittance ratio of 100. *Phys. Rev. ST Accel. Beams* **9**, 031001 (2006).
- Peralta, E. A. *et al.* Demonstration of electron acceleration in a laser-driven dielectric microstructure. *Nature* **503**, 91–94 (2013).
- Breuer, J. & Hommelhoff, P. Laser-based acceleration of nonrelativistic electrons at a dielectric structure. *Phys. Rev. Lett.* **111**, 134803 (2013).
- McNeil, B. W. J. & Thompson, N. R. X-ray free-electron lasers. *Nature Photon.* **4**, 814–821 (2010).
- de Abajo, F. J. G. Multiple excitation of confined graphene plasmons by single free electrons. *ACS Nano* **7**, 11409–11419 (2013).
- Liu, S. *et al.* Coherent and tunable terahertz radiation from graphene surface plasmon polaritons excited by an electron beam. *Appl. Phys. Lett.* **104**, 201104 (2014).
- Jablan, M., Buljan, H. & Soljagic, M. Transverse electric plasmons in bilayer graphene. *Opt. Express* **19**, 11236 (2011).

## Acknowledgements

The authors thank S. Shwartz, H. Buljan and L. Schächter for helpful discussions of aspects related to this work. The work was supported by the US Army Research Laboratory and the US Army Research Office through the Institute for Soldier Nanotechnologies (contract no. W91NF-13-D-0001), and the Science and Engineering Research Council (SERC; grant no.

1426500054) of the Agency for Science, Technology and Research (A\*STAR), Singapore. The research of I.K. was also partially supported by the Seventh Framework Programme of the European Research Council (FP7–Marie Curie IOF) under grant agreement no. 328853 – MC–BSiCS.

#### **Author contributions**

All authors discussed the results and made critical contributions to the work.

#### **Additional information**

Supplementary information is available in the [online version](#) of the paper. Reprints and permissions information is available online at [www.nature.com/reprints](http://www.nature.com/reprints). Correspondence and requests for materials should be addressed to I.K. and L.J.W.

#### **Competing financial interests**

The authors declare no competing financial interests.